ISSN 1560-3547, Regular and Chaotic Dynamics, 2017, Vol. 22, No. 3, pp. 210–225. © Pleiades Publishing, Ltd., 2017.

Autonomous Strange Nonchaotic Oscillations in a System of Mechanical Rotators

Alexey Yu. Jalnine* **and Sergey P. Kuznetsov****

Saratov Branch of Kotel'nikov's Institute of Radio-Engineering and Electronics of RAS
ul. Zelenaya 38, Saratov, 410019 Russia;
Udmurt State University
ul. Universitetskaya 1, Izhevsk, 426034 Russia

Received March 31, 2017; accepted April 18, 2017

Abstract—We investigate strange nonchaotic self-oscillations in a dissipative system consisting of three mechanical rotators driven by a constant torque applied to one of them. The external driving is nonoscillatory; the incommensurable frequency ratio in vibrational-rotational dynamics arises due to an irrational ratio of diameters of the rotating elements involved. It is shown that, when losing stable equilibrium, the system can demonstrate two- or three-frequency quasi-periodic, chaotic and strange nonchaotic self-oscillations. The conclusions of the work are confirmed by numerical calculations of Lyapunov exponents, fractal dimensions, spectral analysis, and by special methods of detection of a strange nonchaotic attractor (SNA): phase sensitivity and analysis using rational approximation for the frequency ratio. In particular, SNA possesses a zero value of the largest Lyapunov exponent (and negative values of the other exponents), a capacitive dimension close to 2 and a singular continuous power spectrum. In general, the results of this work shed a new light on the occurrence of strange nonchaotic dynamics.

MSC2010 numbers: 34C15, 34C28, 34C46, 37C55, 37C70, 37D45, 70K43

DOI: 10.1134/S1560354717030029

Keywords: autonomous dynamical system, mechanical rotators, quasi-periodic oscillations, strange nonchaotic attractor, chaos

1. INTRODUCTION

A *strange nonchaotic attractor* (SNA) is a fundamental type of attractive sets of dynamical systems which manifest a contradictory combination of properties of order and chaos [1]. It possesses a nonsmooth, fractal-like geometrical structure [2, 3] and a singular continuous power spectrum [4–6], but shows no exponential divergence of trajectories and no positive Lyapunov exponents. SNA were first introduced in 1984 (see reference [7]) and since then they have been widely studied theoretically, numerically [8–21] and experimentally [22–27] in relation to nonlinear dynamical systems driven by quasiperiodic external force (e. g., superposition of two and more harmonic signals with fixed irrational frequency ratios). On the other hand, any attempts to observe strange nonchaotic self-oscillations, where the incommensurable frequencies would be produced due to internal properties of the system in the absence of external quasi-periodic forcing, were not successful [28–30]. Thus, the question of the possibility of occurrence of strange nonchaotic self-oscillations remained unsolved.

An example of a self-oscillatory dissipative system of mechanical nature, which manifests strange nonchaotic oscillations operating due to supplied constant torque was first presented in our paper [31]. The model system is composed of three disks 1–3 mounted vertically as shown in Fig. 1. The ratio of radii of the disks 1 and 2 connected through the friction transmission is

*E-mail: Jalnine@rambler.ru
**E-mail: spkuz@yandex.ru

defined by an irrational number $\rho = r_1/r_2$. The condition of motion without slip of the rotating disks is expressed by the relation to the angular coordinates $\theta_2 = \rho\theta_1 + const$ and to the angular velocities $\dot{\theta}_2 = \rho\dot{\theta}_1$. The motion is provided by a constant (not varying in time) torque applied to one of the disks. So the external force is not oscillatory, and the system must be regarded as an autonomous one. Components of the motion with incommensurable frequencies emerge due to a specially selected irrational ratio of sizes of the rotating elements involved. In addition, the disk 1 undergoes viscous friction under rotation, proportional to its angular velocity, and there is also viscous friction between the disks 1 and 3. So the system is dissipative and possesses attractors in the phase space. It was shown that the system can manifest two- and three-frequency quasi-periodic, chaotic and strange nonchaotic types of vibrational and rotational dynamics.

In this paper we expand the results of [31]. We provide extensive theoretical and numerical studies both of the complete (4D) mechanical system and of its reduced (3D) mathematical model. The numerical studies include computation of Lyapunov exponents of the attractors, their fractal dimensions and exponents of phase sensitivity, and a detailed analysis of power spectra of oscillations. We present charts of dynamical regimes in different sections of the parameter space of the model system and dependencies of the Lyapunov exponents on parameters. Based on these results, we analyze dynamical transitions between the dynamical regimes and underline the typicality of certain types of oscillations in the corresponding regions of the parameter space. Results of the present paper shed a new light on the problem of existence of SNA in autonomous systems.

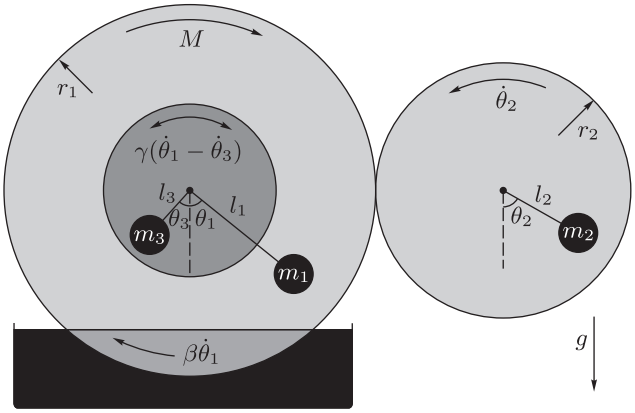

Fig. 1. A schematic image of the mechanical system in which an SNA can be realized.

2. ORIGINAL MECHANICAL SYSTEM AND REDUCED DYNAMICAL MODEL

Let us consider a system of three disks (1, 2, 3), see Fig. 1, two of them are coaxial (1 and 3) and undergo viscous friction, which is proportional to the mutual angular velocity. The motion of the system is provided by constant driving torque applied to the disk 1, whose edges come into contact with those of the disk 2, so that a frictional transmission of rotation occurs without slipping. Besides, the disk 1 undergoes viscous friction itself during rotation proportional to its angular velocity. For simplicity, let us assume that the inertial properties of the system are supplied entirely by the point masses m_1, m_2 and m_3 attached to the disks at distances from the axes, respectively, l_1, l_2 and l_3. In essence, this is a system of pendulums with an imposed mechanical constraint. The relation of radii of the disks 1 and 2 linked by the frictional transmission is supposed to be an irrational number, specifically, we set $\rho = r_1/r_2 = (\sqrt{5}+1)/2$. Taking into account the relationships $\theta_2 = \rho\theta_1 + u$ and $\dot{\theta}_2 = \rho\dot{\theta}_1$, we can write the Lagrangian function of the system as one depending only on the angle coordinates $\theta_{1,3}$ and velocities $\dot{\theta}_{1,3}$:

$$L = \frac{1}{2}m_1 l_1^2\dot{\theta}_1^2 + \frac{1}{2}m_2 l_2^2\rho^2\dot{\theta}_1^2 + \frac{1}{2}m_3 l_3^2\dot{\theta}_3^2 + m_1 l_1 g\cos\theta_1 + m_2 l_2 g\cos(\rho\theta_1 + u) + m_3 l_3 g\cos\theta_3. \tag{2.1}$$

Introducing a dissipation with the help of the Rayleigh function

$$R = \frac{1}{2}\gamma_0(\dot\theta_1 - \dot\theta_3)^2 + \frac{1}{2}\beta_0\dot\theta_1^2 - M_0\dot\theta_1,$$

we obtain equations of motion in the form [32]:

$$\frac{d}{dt}\left(\frac{\partial L}{\partial \dot\theta_i}\right) = \frac{\partial L}{\partial \theta_i} - \frac{\partial R}{\partial \dot\theta_i}, \qquad i = 1, 3,$$

or

$$\begin{aligned}(m_1 l_1^2 + m_2 l_2^2\rho^2)\ddot\theta_1 &= -m_1 l_1 g\sin\theta_1 - m_2 l_2 g\rho\sin(\rho\theta_1 + u) + \gamma_0\dot\theta_3 - (\beta_0 + \gamma_0)\dot\theta_1 + M_0,\\ m_3 l_3^2\ddot\theta_3 &= -m_3 l_3 g\sin\theta_3 + \gamma_0(\dot\theta_1 - \dot\theta_3).\end{aligned}$$

Using the notation $\theta = \theta_1$, $\varphi = \theta_3$, the dimensionless time $\tau = t\sqrt{m_1 l_1 g/(m_1 l_1^2 + m_2 l_2^2\rho^2)}$ and the dimensionless parameters

$$\begin{aligned}&\gamma = \frac{\gamma_0}{\sqrt{m_1 l_1 g(m_1 l_1^2 + m_2 l_2^2\rho^2)}}, \qquad \beta = \frac{\beta_0}{\sqrt{m_1 l_1 g(m_1 l_1^2 + m_2 l_2^2\rho^2)}},\\ &\lambda_2 = \frac{m_2 l_2}{m_1 l_1\rho}, \quad \lambda_3 = \frac{m_3 l_3}{m_1 l_1\rho}, \qquad \mu = \frac{m_3 l_3^2}{m_1 l_1^2 + m_2 l_2^2\rho^2}, \quad M = \frac{M_0}{m_1 l_1 g},\end{aligned} \tag{2.2}$$

we arrive at the following equations:

$$\begin{aligned}\ddot\theta &= -\sin\theta - \lambda_2\sin(\rho\theta + u) + \gamma\dot\varphi - (\beta + \gamma)\dot\theta + M,\\ \mu\ddot\varphi &= -\lambda_3\sin\varphi + \gamma(\dot\theta - \dot\varphi).\end{aligned} \tag{2.3}$$

Under the condition $\mu \ll 1$ the system of equations can be reduced and rewritten in the form:

$$\begin{aligned}\dot\theta &= \omega,\\ \dot\omega &= -\sin\theta - \lambda_2\sin(\rho\theta + u) - \lambda_3\sin\varphi - \beta\omega + M,\\ \dot\varphi &= -\lambda_3\gamma^{-1}\sin\varphi + \omega.\end{aligned} \tag{2.4}$$

3. ATTRACTORS OF THE MODEL SYSTEM AND THEIR CHARACTERISTICS

Let us study the system (2.4) with fixed parameters $\lambda_3 = 1$, $\beta = 1$, $\gamma = 1$, $\rho = (\sqrt{5}+1)/2$, while λ_2 and M are supposed to be varied.

In Fig. 2 examples of the Poincaré sections for attractors of the system (2.4) are shown. The cross-sections are assumed at the moments corresponding to increase of θ by 2π, namely, $\theta_n = \theta_0 + 2\pi n, n = 1\ldots 10^6$, with $\theta_0 = 0.0$. The first column presents the attractors in coordinates $(\omega_n, \dot\omega_n)$, while the second one shows them in coordinates (ξ_n, ω_n), where $\xi_n = \rho\theta_n \pmod{2\pi}$.

The attractor in Fig. 2a is a two-frequency torus; it corresponds to a smooth closed invariant curve in the Poincaré section. Figure 2b shows a three-frequency torus; its section gives rise to a smooth 2D surface. The attractors in Figs. 2c and 2d are strange, and for their confident identification one needs calculation of dynamical and metrical characteristics as Lyapunov exponents, phase sensitivity exponents, and fractal dimensions.

Computations of the Lyapunov exponents were performed with the Benettin algorithm [33] using the equations linearized near a reference phase trajectory of the system (2.4):

$$\begin{aligned}\dot{\tilde\theta} &= \tilde\omega,\\ \dot{\tilde\omega} &= -\tilde\theta\cos\theta - \lambda_2(\rho\tilde\theta + \tilde u)\cos(\rho\theta + u) - \lambda_3\tilde\varphi\cos\varphi - \beta\tilde\omega,\\ \dot{\tilde\varphi} &= -\lambda_3\gamma^{-1}\tilde\varphi\cos\varphi + \tilde\omega.\end{aligned} \tag{3.1}$$

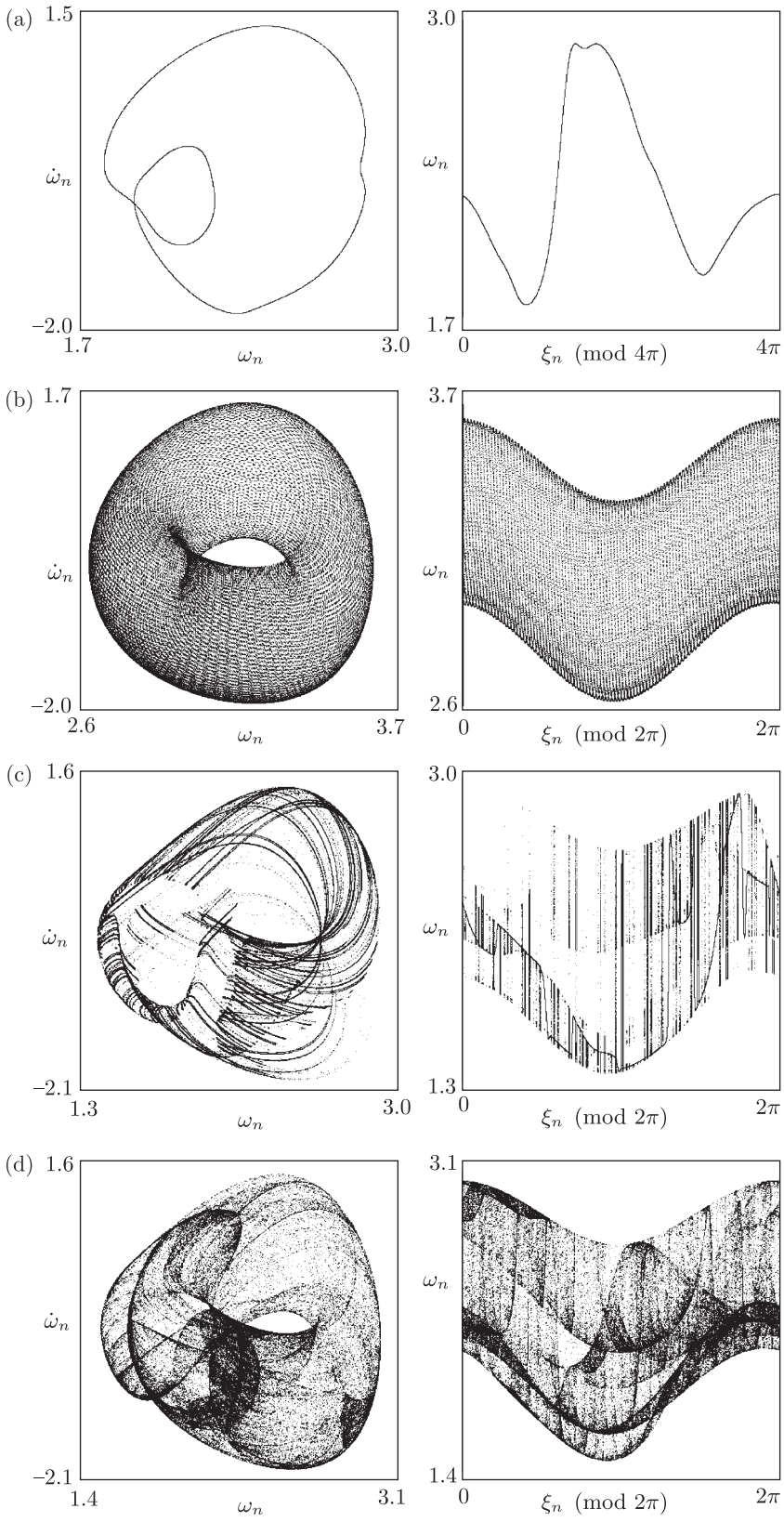

Fig. 2. Phase portraits of attractors in projection to the plane in the Poincaré section $\theta \pmod{2\pi} = 0$ for $\lambda_2 = 0.8$: (a) $M = 2.3$ is a two-dimensional torus with a closed invariant curve in section; (b) $M = 3.0\ 0$ is a three-dimensional torus; (c) $M = 2.1$ is an SNA; (d) $M = 2.2$ is a chaotic attractor.

A set of three copies of Eqs. (3.1) with vectors of variables $\{\tilde{\theta}^{(k)}, \tilde{\omega}^{(k)}, \tilde{\varphi}^{(k)}\}_{k=1,\ldots,3}$ and $\tilde{u}^{(k)} = 0$ are integrated numerically simultaneously with the system (2.4); the procedure is complemented by renormalization via the Gram – Schmidt procedure after equal time intervals; logarithms of the normalization coefficient were summarized and averaged, finally resulting in the estimate of the three Lyapunov exponents.

For the two-frequency torus in Fig. 2a the Lyapunov exponents are $\Lambda_1 = 0 \pm 10^{-5}$, $\Lambda_2 = -0.0979$, $\Lambda_3 = -0.798$, and for the three-frequency torus in Fig. 2b they are $\Lambda_1 = 0 \pm 10^{-5}$, $\Lambda_2 = 0 \pm 10^{-5}$, $\Lambda_3 = -0.937$. The attractor in Fig. 2c is characterized by the set $\Lambda_1 = 0 \pm 10^{-5}$, $\Lambda_2 = -0.105$, $\Lambda_3 = -0.894$, which testifies to its nonchaotic nature, although the geometrical structure looks quite unlike a smooth invariant curve or surface. Finally, the chaotic attractor in Fig. 2d is characterized by a set of exponents, one of which is positive: $\Lambda_1 = 0.0206$, $\Lambda_2 = 0 \pm 10^{-5}$, $\Lambda_3 = -0.869$.

Note that in all the cases there is one more trivial exponent, which is associated with the variable $\xi = \rho\theta + u$ and with the equation $\dot{\tilde{\xi}} = \rho\tilde{\omega}$, which can be added to the system (3.1). We do not mention it with respect to the procedure of the exponents computation, but keep it in mind for retaining classical signatures of Lyapunov exponents.

The characteristic power spectra for all corresponding self-oscillation regimes are presented in Fig. 3. The spectra for two- and three-frequency oscillations look like discrete sets of peaks at certain frequencies (Figs. 3a, 3b), while for the chaotic mode the spectrum is continuous (Fig. 3d). As for the case of a strange nonchaotic attractor (Fig. 3c), the spectrum possesses a combination of features of order and chaos: one can observe a set of well-expressed characteristic peaks, which looks dense on the frequency axis, but there is also a "substrate", which makes the spectral density nonvanishing outside the peaks.

Following [4–6], to characterize spectra in more detail, consider the spectral sums $Z(\Omega, m)$:

$$Z(\Omega, m) = \sum_{k=0}^{m-1} \omega_k e^{i2\pi k\Omega},$$

where $\{\omega_k\}_{k=0,\ldots,m-1}$ is a sequence of values of a dynamical variable produced by the Poincaré map, and m is the total number of the points.

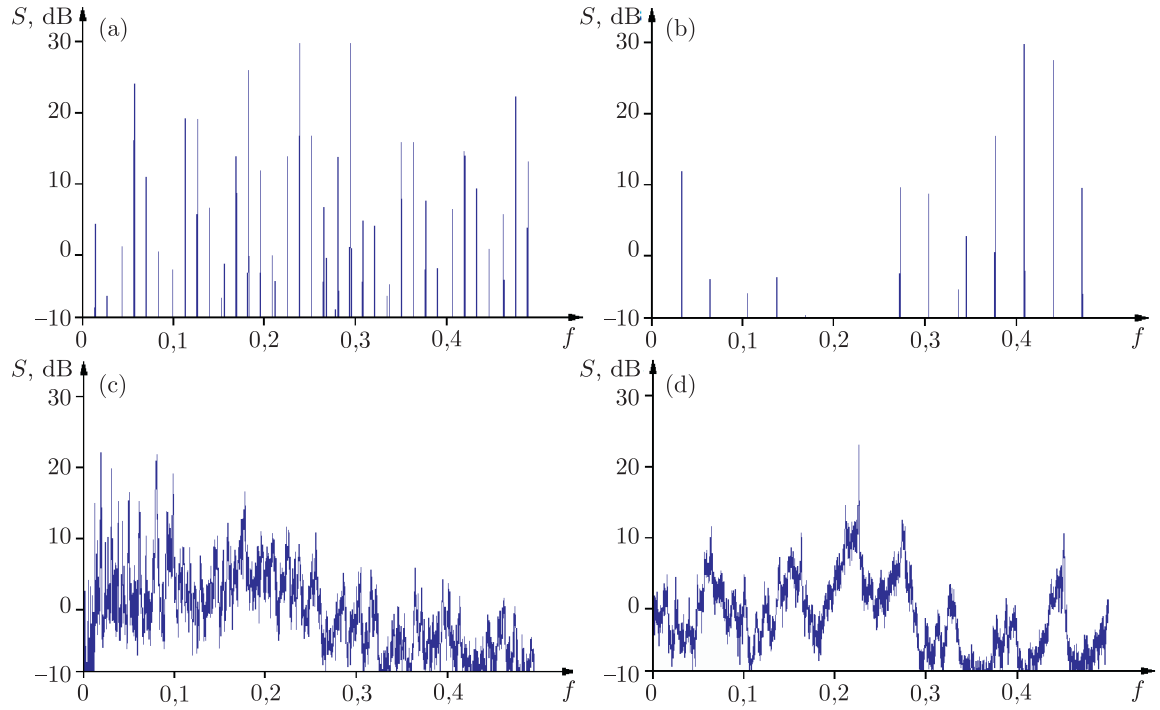

Fig. 3. Spectra calculated via discrete (at $\theta \pmod{2\pi} = 0$) sequence $\{\omega_n\}$ for the system (2.4) for $\lambda_2 = 0.8$: (a) $M = 2.3$, two-frequency quasiperiodicity; (b) $M = 3.0$, three-frequency quasiperiodicity; (c) $M = 2.1$, SNA; (d) $M = 2.2$, chaos.

As is well known, discrete spectra corresponding to periodic and quasi-periodic modes consist of countable sets of frequency components with nonzero amplitudes. Their spectral sums accumulate as $|Z|^2 \sim m^2$ at the frequencies presented in the spectrum, or they do not grow in absolute value if the parameter Ω corresponds to a frequency absent in the spectrum. For chaotic and stochastic regimes and signals, the point on the complex plane, presenting a spectral sum, performs random walking, which corresponds to a linear growth of the averaged squared value of the spectral sum modulus as $|Z|^2 \sim m$; it occurs for all or almost all values of the frequency parameter Ω. Such spectra are regarded as "continuous" and are considered in the framework of the Wiener – Khinchin theory. As for the SNA, singular continuous spectra are intrinsic to them [4, 5], where the growth of the spectral sums is characterized by nontrivial fractional exponents.

Figure 4 shows diagrams of $|Z(\Omega, m)|^2$ depending on m for different Ω (the first row of diagrams), and the walking of the complex value of the spectral sums on the complex plane (the second row) for SNA at $M = 2.1$. The maximum trajectory length is 10^7 points; in order to obtain an exponent of sum growth, a linear approximation via the least-squares method was used along 30 points with numbers given by the Fibonacci numbers (from $F_6 = 8$ to $F_{35} = 9227465$). The diagrams are presented on a double logarithmic scale.

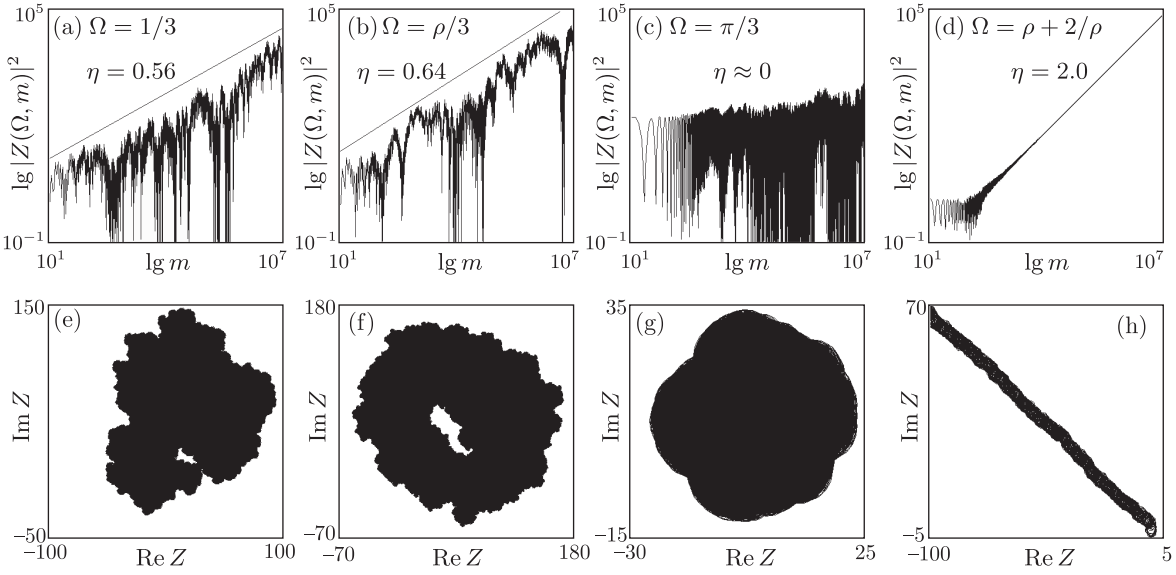

Fig. 4. Plots of dependencies of the squared spectral sum $|Z(\Omega, m)|^2$ for different frequency values: (a) $\Omega = 1/3$, (b) $\Omega = \rho/5$, (c) $\Omega = \pi/3$, (d) $\Omega = \rho + 2/\rho$. Walks of the image point of the spectral sum on the complex plane: (e), (f), (g), (h) at the same frequencies.

Numerical analysis reveals a few characteristic types of the spectral sums behavior with growth of m. For randomly chosen rational (Fig. 4a) and irrational (Fig. 4b) frequencies, the value of $|Z|^2$ grows via a power law $|Z(\Omega, m)|^2 \sim m^\eta$ with exponent $0 \leqslant \eta < 1$. In some cases, the growth of the spectral sums does not take place or may be so slow that it can hardly be resolved in the computations (Fig. 4c). On the other hand, there exists a set of frequencies which manifests the growth of spectral sums via the law characteristic for a quasi-periodic dynamics: $|Z(\Omega, m)|^2 \sim m^2$. Empirically we found that the corresponding frequencies could be expressed as

$$\Omega = \sum_i a_i \rho^{b_i}, \tag{3.2}$$

where a_i and b_i are arbitrary integers (both positive and negative), and the number of terms in the sum (3.2) is not restricted. A characteristic example of such behavior of spectral sums is presented in Fig. 4d for $\Omega = \rho + 2/\rho$. Note that frequencies equal modulo 1 provide identical exponents of growth; so, the relation frequencies (3.2) determine a dense set of spectral peaks on the unit interval of the frequency axis.

The lower row of diagrams in Fig. 4 illustrates random walks of the image point of the spectral sum on the complex plane. This walking looks like a random diffusion for the cases of fractional values of the exponent of spectral sum growth, and it turns out to be a directed drift for frequencies given by the formula (3.2).

It is necessary to note that the obtained results are somewhat different from the ones presented in references [4–6] for singular continuous spectra, since in the cited works the exponents of spectral sums growth turn out to be localized within the interval $1 < \eta \leqslant 2$, i. e., between well-ordered growth and chaotic diffusion. Apparently, in the general case the distributions of amplitudes of spectral components in systems with SNA may obey more complex rules than the ones typical for the specific discrete model examined in the mentioned works[1)].

In order to exactly identify SNA and distinguish it from a two-dimensional torus (which is characterized by the same signature of Lyapunov exponents: $\{0, -, -\}$), we make use of two methods suggested in reference [10].

The first method, known as the "rational frequency approximation", is to replace the irrational parameter ρ by rational approximants $\{\rho_k\}$ such that $\rho = \lim_{k\to\infty} \rho_k$. For the "golden mean" value of ρ the ratios of Fibonacci numbers ($\rho_k = F_{k+1}/F_k$, $F_{k+1} = F_k + F_{k-1}$, $F_1 = 1$, $F_2 = 1$) are the approximants. At the k-th step of approximation, instead of the single system (2.4) with irrational ρ, we consider an ensemble of analogous systems with rational ρ_k. In this case, one can choose various values of the initial angle u, which becomes a relevant parameter of the system. Under variation of the initial angle within the interval $u \in [0, 2\pi/F_k]$, the range of the variable $\xi \pmod{2\pi}$ fills the whole interval $[0, 2\pi]$, and the set of orbits corresponding to different values of u composes the whole approximation of the attractor of the original system. It is assumed that the properties of the original system will be obtained in the limit $k \to \infty$. In the case where the original attractor is a smooth torus, its approximation is also a closed smooth invariant set consisting of stable cycles of period F_k with no bifurcation points. If any bifurcations of orbits occur under variation of the initial angle u, it makes the approximating set nonsmooth and thus indicates a "strange" geometry of the attractor being approximated. The existence of bifurcations of approximating orbits at different levels k of approximation and the persistence of bifurcations under increase of the approximation precision is a sufficient condition for the existence of SNA. For different values of F_k and of the initial angle u, the approximating set for the SNA may contain periodic orbits of different periods (divisible by F_k), quasi-periodic and chaotic orbits.

Figure 5 illustrates the structure of the approximating sets for the SNA at parameters of Fig. 2c and for different rational approximants $8/5, 13/8, 34/21, 55/34, 89/55, 144/89$. Each horizontal row of diagrams (a), (b), …, (f) corresponds to one and the same value of ρ_k.

Consider first the upper row (a), which corresponds to $\rho_k = 8/5$. The first diagram presents a Poincaré section of the approximating set of orbits in coordinates $(\omega_n, \dot{\omega}_n)$. As previously, the section is performed at the moments $\theta = 0 \pmod{2\pi}$, with the initial angle u for orbits being varied uniformly within the interval $u \in [0, 2\pi/F_k]$. Then the values of $\xi_n = 2\pi\rho_k n + u \pmod{2\pi}$ fill the whole interval $[0, 2\pi]$. In the second and third diagrams the Poincaré sections on the plane of variables (ξ_n, ω_n) are presented; note that in the third diagram the variable ξ_n possesses values within the interval $\xi_n \in [0, 2\pi/F_k]$, which allows one to discern the internal bifurcation structure of the approximating set. In these diagrams one can observe cascades of period doubling bifurcations and transitions to chaos, so that the whole approximation of the attractor represents an aggregate of periodic and chaotic orbits. The existence of bifurcations and chaos is also confirmed by plots of Lyapunov exponents versus u, as shown in the last diagram of the row. At the moment of bifurcation the second exponent Λ_2 takes zero value, and in the chaotic regions the largest exponent Λ_1 is positive.

The posterior rows of diagrams ((b), (c) etc.) illustrate the approximating sets of orbits for the SNA at higher levels k of the approximation. In these diagrams one can see that the bifurcations persist under increase of the approximation number, while the structure of the bifurcation sets

[1)] Besides the model system (2.4), the properties of spectral sums for the "robust" strange nonchaotic attractor in the system of Hunt and Ott (see map (1) in reference [3]) were also investigated in the course of our studies. The results we obtained turned out to be identical to the ones presented here for the system (2.4), which testifies to the existence of a more general pattern of spectral structure for SNA, which is not connected to our specific choice of the model system.

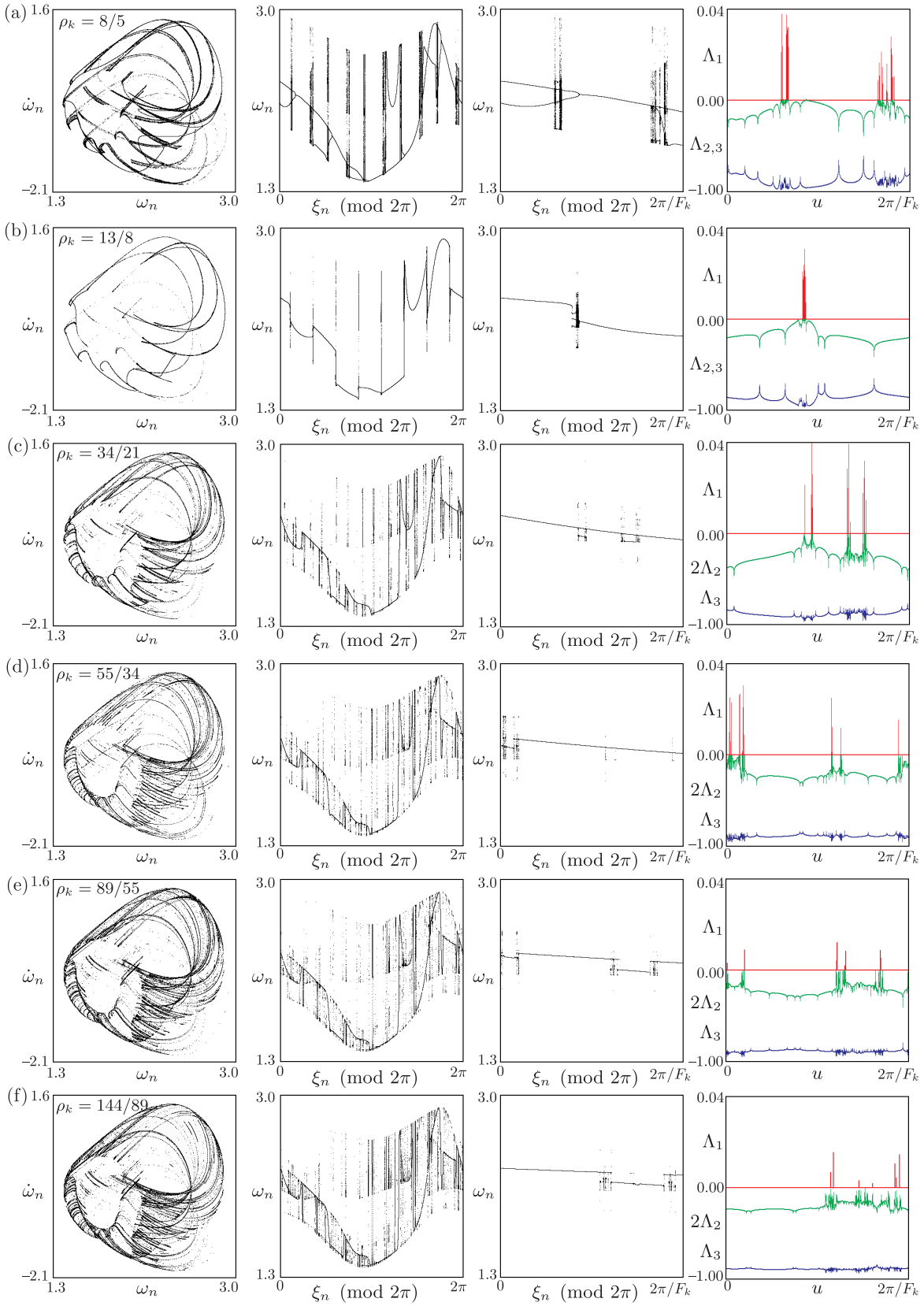

Fig. 5. Rational approximation of SNA for $\lambda_2 = 0.8$, $M = 2.1$ and different ρ_k. (a): $\rho_5 = 8/5$, (b): $\rho_6 = 13/8$, (c): $\rho_8 = 34/21$, (d): $\rho_9 = 55/34$, (e): $\rho_{10} = 89/55$, (f): $\rho_{11} = 144/89$. See explanations in the text.

becomes more complicated; breaks of the curves at the bifurcation points are visible. Also, the number of chaotic orbits within the approximating set decreases, which agrees with the existence of the nonchaotic limiting attractor. Summing up, such a structure of approximation, persisting under increase of the approximation accuracy, suggests that the structure of the attractor is nonsmooth as $\rho_k \to \rho$, which is what we set out to show.

The second method for distinguishing SNA from a smooth torus is to analyze the phase sensitivity. To use this method, we introduce a nonzero infinitesimal phase shift $\tilde{u} = \text{const} \neq 0$ in the linearized system (3.1). After that, Eqs. (3.1) are integrated together with (2.4) and with the initial conditions $\tilde{\theta}(0) = 0$, $\tilde{\omega}(0) = 0$, $\tilde{\varphi}(0) = 0$ and $\tilde{u}(0) = 1$. Define now a piecewise smooth function as the magnitude of the maximal variation of the variables along the orbit segment, namely, $\Gamma_{max}(T) = \max_{t\in[0,T]} \sqrt{\tilde{\theta}^2(t) + \tilde{\omega}^2(t) + \tilde{\varphi}^2(t)}$. Next, we introduce the phase sensitivity function as a minimum of the functions $\Gamma_{max}(T)$ computed along a set of N trajectories with randomly specified initial conditions: $\Gamma(T) = \min_{(\theta_n(0),\omega_n(0),\varphi_n(0))_{n=1,\dots,N}} \Gamma_{max}(T)$. It is known that the function of the phase sensitivity is bounded when the attractor is a smooth torus, and grows without limit, according to a power law $\Gamma(T) \propto T^{\delta}$, where $\delta > 0$ is the index of the phase sensitivity, in the case of SNA [10]. Typical plots of $\Gamma(T)$ for a smooth two-frequency torus ($\delta = 0$) and for an SNA ($\delta = 1.7$) are shown in Fig. 6a. The parameter values are the same as in Figs. 2a, 2c.

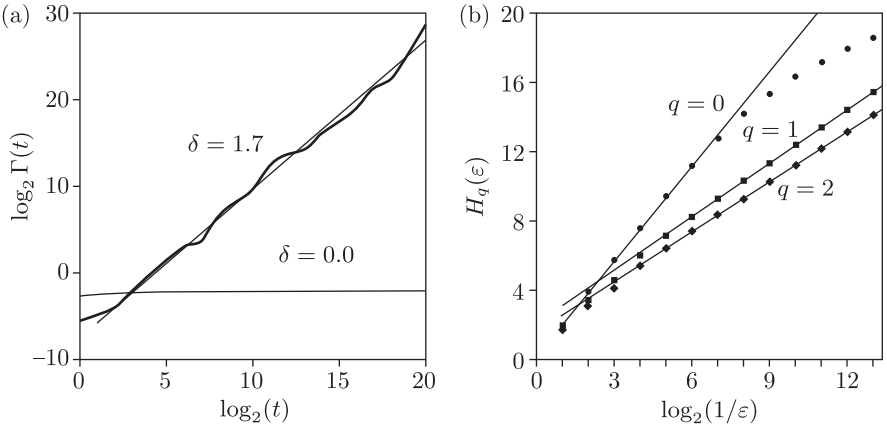

Fig. 6. (a) Plot of the phase sensitivity function for the SNA mode ($\delta = 1.7$) and for the 2D smooth torus ($\delta = 0$). (b) The dependence of Renyi entropy $H_q(\varepsilon)$ on the partition scale ε for $q = 0, 1, 2$.

Direct verification of the "strange" geometric structure of the attractor can be performed by calculating the fractal dimensions [34]. The spectrum of generalized dimensions is introduced via the Renyi entropy values $H_q(\varepsilon)$ depending on the parameter q:

$$H_q(\varepsilon) = \frac{1}{1-q} \log \left(\sum_{i=1}^{N(\varepsilon)} p_i^q \right), \quad D_q = -\lim_{\varepsilon \to 0} \frac{H_q(\varepsilon)}{\log \varepsilon}. \tag{3.3}$$

Here ε is the size of elements covering the attractor and p_i is the measure (probability of visiting) attributed to the i-th element. With $q = 0, 1$, and 2 we get the capacitance, information[2)] and correlation dimension, respectively. It is believed [2, 3] that the dimensions for the strange nonchaotic attractor are

$$D_0 = 2, \quad D_1 = 1, \quad D_2 < 1.$$

To calculate the dimensions, we use the Poincaré section for trajectories on the attractor at $\theta_n = \theta_0 + 2\pi n$, $n = 1, \dots, 10^7$. Next, for given $q = 0, 1, 2$ we plot the Renyi entropies $H_q(\varepsilon)$ versus ε and select linear parts of the plots there (see. Fig. 6b); the slope coefficients just yield the respective fractal dimensions. Specifically, we have obtained $D_0 = 1.8$, $D_1 = 1.02$, and $D_2 = 0.96$. This reasonably agrees with the estimations in references [2, 3].

[2)] It should be noted that with $q = 1$ the l'Hopital rule has to be applied in formula (3.3) to exclude the uncertainty.

4. PARAMETER SPACE STRUCTURE AND DYNAMICAL TRANSITIONS OF THE REDUCED MODEL

Let us consider the problem of the existence of a stable equilibrium and of a vibrational-rotational dynamics in the model system (2.4). For this, we require the right-hand sides of the equations to be zero. From the second equation we obtain the relation $\sin\theta + \lambda_2 \sin(\rho\theta + u) = M$. It immediately follows that for $M > \lambda_2 + 1$ the stable equilibrium cannot occur in the mechanical system. Therefore, the dynamics of the system must be rotational, with the phase increasing with time.

Figure 7a gives a general idea of the parameter space structure for the system (2.4). In this figure a fragment of a chart of dynamical regimes is presented on the parameter plane in the region of nontrivial dynamics. Blue indicates the areas of two-frequency quasi-periodic oscillations (2T), green indicates the three-frequency quasi-periodicity (3T), yellow means the strange nonchaotic attractor (SNA), and red corresponds to the chaotic attractor (CA). In the white area below the line $M = \lambda_2 + 1$, the attractor is a trivial stable equilibrium (SE) point. Note that vibrational-rotational dynamical regimes can exist in the region $M < \lambda_2 + 1$ also, jointly with the stable equilibrium. They can arise for appropriate choices of initial conditions. Such a phenomenon is known as "multistability". Figure 7b shows an enlarged fragment of the chart in the region of complex dynamical transitions between "regular" and "strange" regimes (the colors have the same meaning, as previously). These charts show a wide range of all basic types of dynamical behavior in the parameter space of our model.

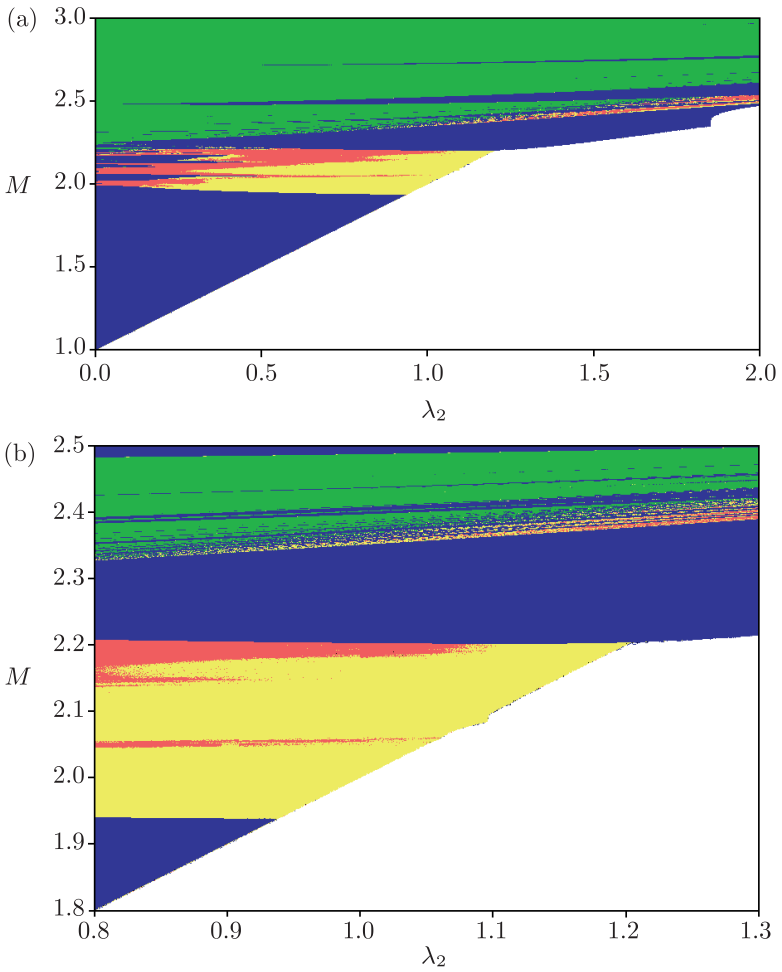

Fig. 7. (a) A fragment of the chart of dynamical regimes for the system (2.4). (b) The enlarged fragment of the chart in the region of complex dynamical transitions.

Let us fix the parameter value $\lambda_2 = 0.8$ and analyze the dynamical transitions under increase of the driving torque M. Moving along the left cut of the parameter plane chart in Fig. 7b, one can observe the following sequence of the alternating dynamical regimes: SE→2T→SNA→CA→2T→3T. Let us consider them in some detail. The transition SE→2T occurs due to a backward saddle-node bifurcation of the stable equilibrium point, and then a two-frequency quasi-periodic rotational mode arises. Under further increase of the moment M, a two-frequency torus breaks down with the birth of the strange nonchaotic attractor (2T→SNA). In its turn, the regions of SNA alternate with chaos until the next saddle-node bifurcation occurs, and a new two-frequency attracting torus arises (CA→2T). Under further increase of M, one can observe an infinite sequence of forward and backward saddle-node bifurcations of tori when crossing the Arnold tongues of synchronization, so that the regimes of two- and three-frequency quasi-periodicity alternate at a small variation scale of M.

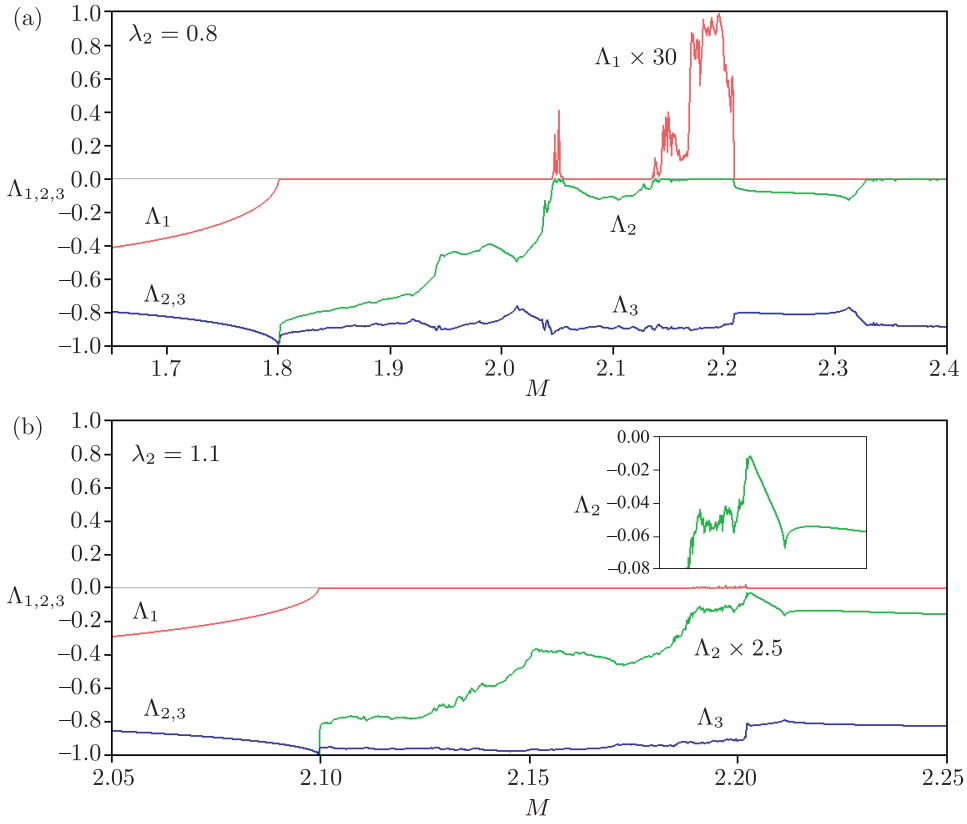

Fig. 8. Plots of the dependencies of Lyapunov exponents on the parameter M for (a) $\lambda_2 = 0.8$, (b) $\lambda_2 = 1.1$.

In Fig. 8a the corresponding plots of Lyapunov exponents versus the parameter M are shown. These plots also make it possible to distinguish intervals of the stable equilibrium ($\Lambda_{1,2,3} < 0$), two-frequency quasi-periodicity or SNA ($\Lambda_1 = 0$, $\Lambda_{2,3} < 0$), three-frequency quasi-periodicity ($\Lambda_{1,2} = 0$, $\Lambda_3 < 0$), chaos ($\Lambda_1 > 0$, $\Lambda_2 = 0$, $\Lambda_3 < 0$). Moreover, based on the values of Lyapunov exponents at dynamical transitions, we can also suggest whether they are smooth (phase-independent) or nonsmooth (phase-dependent)[3)]. At the moment of a smooth transition, the largest nontrivial Lyapunov exponent takes zero value, as it occurs at the transitions SE→2T ($\Lambda_1 = 0$), CA→2T

[3)] By "smooth" one means bifurcations of a torus when all of the quasi-periodic orbits on the torus transform simultaneously, irrespective of their phase coordinate on the torus; for example, this occurs at a smooth saddle-node bifurcation, when the stable torus uniformly collides with the saddle one. When the "nonsmooth", phase-dependent bifurcation takes place, the collision occurs in the dense set of points on the torus. Smooth and nonsmooth bifurcations of tori are considered in detail in reference [16]; the corresponding renormalization group analysis is carried out in reference [17].

($\Lambda_{1,2} = 0$) and 2T→3T ($\Lambda_2 = 0$). On the other hand, the transition 2T→SNA is a nonsmooth one, since it is accompanied by a nonzero value of the largest nontrivial Lyapunov exponent ($\Lambda_2 < 0$); as for the transition SNA→CA, it has a statistical nature [35]. In Fig. 8b, analogous plots are presented for $\lambda_2 = 1.1$. Note that the transition SNA→2T in Fig. 8b also occurs due to the phase-dependent mechanism, since the corresponding exponent is nonzero ($\Lambda_2 < 0$, see the enlarged fragment of the plot).

5. ATTRACTORS AND DYNAMICAL TRANSITIONS IN THE ORIGINAL MECHANICAL SYSTEM

So far, we have considered numerically the reduced (3D) system (2.4). In this section we return to the original (4D) mechanical system described by Eqs. (2.3). Our aim is to discuss the correspondence between these models and to ascertain how the reduction of the model has affected the range of the dynamical phenomena being observed. We proceed from the assumption that the reduction of the original equations does not play an essential role and does not result in the appearance of any new dynamics that are not typical of the realistic mechanical system.

First, let us choose the value of a "small" parameter $\mu = 0.1$, while the other parameters will remain the same ($\lambda_3 = 1$, $\beta = 1$, $\gamma = 1$, $\rho = (\sqrt{5}+1)/2$), and the parameters λ_2 and M are varied. The system (2.3) can be rewritten as

$$\begin{aligned} &\dot\theta = \omega,\\ &\dot\omega = -\sin\theta - \lambda_2 \sin(\rho\theta + u) + \gamma\psi - (\beta+\gamma)\omega + M,\\ &\dot\varphi = \psi,\\ &\dot\psi = \mu^{-1}\big(-\lambda_3 \sin\varphi + \gamma(\omega - \psi)\big). \end{aligned} \tag{5.1}$$

Figure 9 shows examples of the attractors of the system: two- and three-dimensional tori, strange nonchaotic and chaotic attractors. The characteristic Lyapunov exponents were calculated, as previously, by linearizing the system (5.1) and using the Benettin algorithm. They are:
(a) $\Lambda_1 = 0 \pm 10^{-5}$, $\Lambda_2 = -0.0472$, $\Lambda_3 = -0.7225$, $\Lambda_4 = -11.23$;
(b) $\Lambda_1 = 0 \pm 10^{-5}$, $\Lambda_2 = 0 \pm 10^{-5}$, $\Lambda_3 = -0.8439$, $\Lambda_4 = -11.16$;
(c) $\Lambda_1 = 0 \pm 10^{-5}$, $\Lambda_2 = -0.0583$, $\Lambda_3 = -0.7921$, $\Lambda_4 = -11.15$;
(d) $\Lambda_1 = 0.0247$, $\Lambda_2 = 0 \pm 10^{-5}$, $\Lambda_3 = -0.7852$, $\Lambda_4 = -11.24$.

The power spectra for the corresponding oscillatory regimes at the same parameter values are shown in Fig. 10. The spectra have characteristic discrete peaks for two- and three-frequency quasi-periodic regimes (Figs. 10a, 10b). For the chaotic mode, the power spectrum is continuous (Fig. 10d), and for the strange nonchaotic self-oscillatory regime it has more complicated (singular continuous) structure (Fig. 10c).

In order to characterize and distinguish SNA from a 2D smooth torus, we use the method of phase sensitivity in the same way as in Section 3 for the reduced system. Namely, we introduce the phase sensitivity function as $\Gamma_{max}(T) = \max_{t\in[0,T]}(\tilde\theta^2(t) + \tilde\omega^2(t) + \tilde\varphi^2(t) + \tilde\psi^2(t))^{-1/2}$ and $\Gamma(T) = \min_{(\theta_n(0),\omega_n(0),\varphi_n(0),\psi_n(0))_{n=1,\dots,N}} \Gamma_{max}(T)$. The value of the phase sensitivity exponent for the SNA at $\lambda_2 = 0.8$ and $M = 2.0$ turns out to be $\delta \approx 2.6$; for the case of a 2D torus at $\lambda_2 = 0.8$ and $M = 2.15$ the function $\Gamma(T)$ is bounded ($\delta = 0.0$), see Fig. 11a. A direct check of the dynamical and metrical characteristics of the SNA via calculation of the generalized dimensions shows the existence of a fractal-like structure: the attractor possesses values of capacity dimension $D_0 \approx 1.9$, information dimension $D_1 \approx 1.1$ and correlation dimension $D_2 \approx 0.97$ (see Fig. 11b), which agrees well with the previously reported results of references [2, 3]. Thus, one can conclude that the original system (5.1) possesses the same basic types of self-oscillatory dynamical regimes (and the corresponding attractors in the phase space) as the reduced system (2.4).

Finally, let us consider the structure of the parameter space of the system (5.1) in different sections. Figure 12 shows two different charts of dynamical regimes: on the plane (λ_2, M) at $\mu = 0.1$ (Fig. 12a) and on the plane (μ, M) at $\lambda_2 = 0.8$ (Fig. 12b).

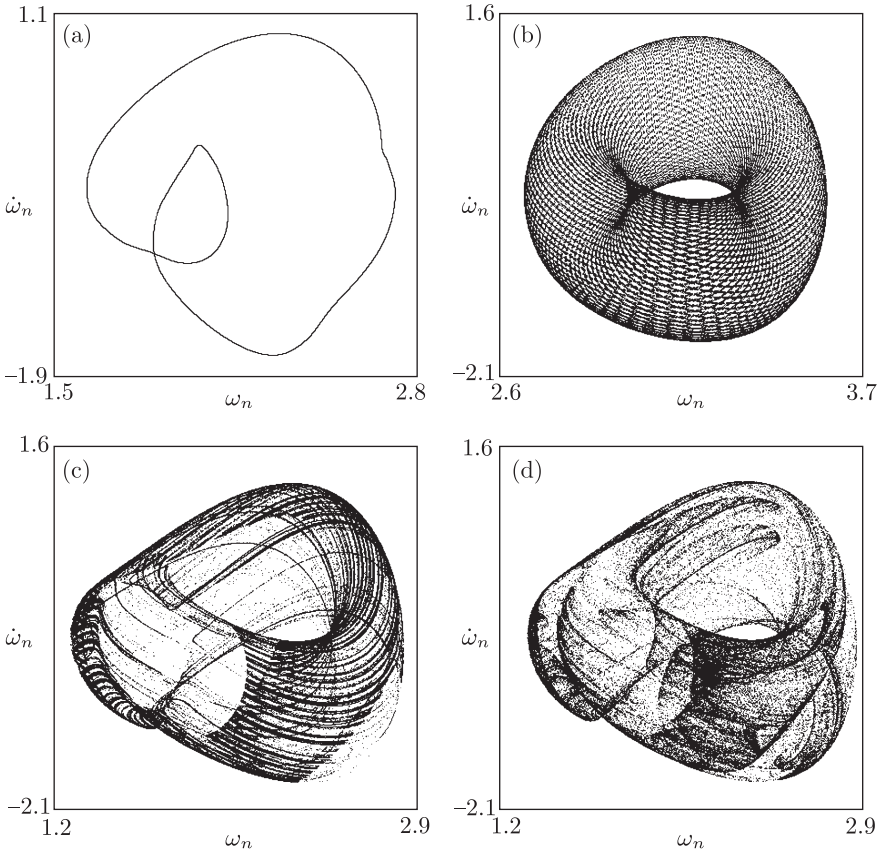

Fig. 9. Phase portraits of the attractors of the system (5.1) in the Poincaré section at $\theta \pmod{2\pi} = 0$ for $\lambda_2 = 0.8$: (a) 2D torus at $M = 2.15$ (closed invariant curve); (b) 3D torus at $M = 3.0$; (c) SNA at $M = 2.0$; (d) chaotic attractor at $M = 2.04$.

Comparing the charts of dynamical regimes in Fig. 12a and in Fig. 7b, one can see a similar structure of the regions of different dynamics for the fixed small parameter $\mu = 0.1$. First, as previously, the stable equilibrium of the system is possible only in the region $M < \lambda_2 + 1$, which can be checked by setting to zero the right-hand sides of all equations of the system (5.1). Also, the vibrational-rotational dynamics is possible in this region under appropriate initial conditions, so that the multistability may take place. Second, the displacement of the system from equilibrium may lead either to two-frequency quasi-periodic or to strange nonchaotic and chaotic dynamics. Third, as before, the three-frequency quasi-periodicity arises as the torque M increases, and it predominates in the parameter space over all other possible dynamical regimes.

The second chart (in Fig. 12b) shows how the set of basic regimes changes as the parameter μ increases. It immediately follows from this chart that nontrivial types of dynamics (i.e., SNA and chaos) mainly exist in the region $\mu < 0.3$. For larger values of the parameter μ the dynamics of the system degenerates into two- and (mainly) three-frequency quasi-periodicity. Taking into account the physical meaning of the parameter μ (see Fig. 1 and formulas (2.2)), one can conclude that the mechanical system exhibits nontrivial behavior at relatively small values of: (i) the torque affecting the disk 1, and (ii) the size of the disk 3 and the mass concentrated on it.

6. CONCLUSION

In conclusion, we note that the interest in "strange" and complex dynamics of self-oscillatory systems is not incidental. The investigation of such systems is of theoretical and especially practical importance. Self-generators may be preferable compared to forced generators in some practical applications where a synchronization of subsystems is required, e.g., in secure communication, since the absence of an external driving force simplifies the procedure of synchronization of the

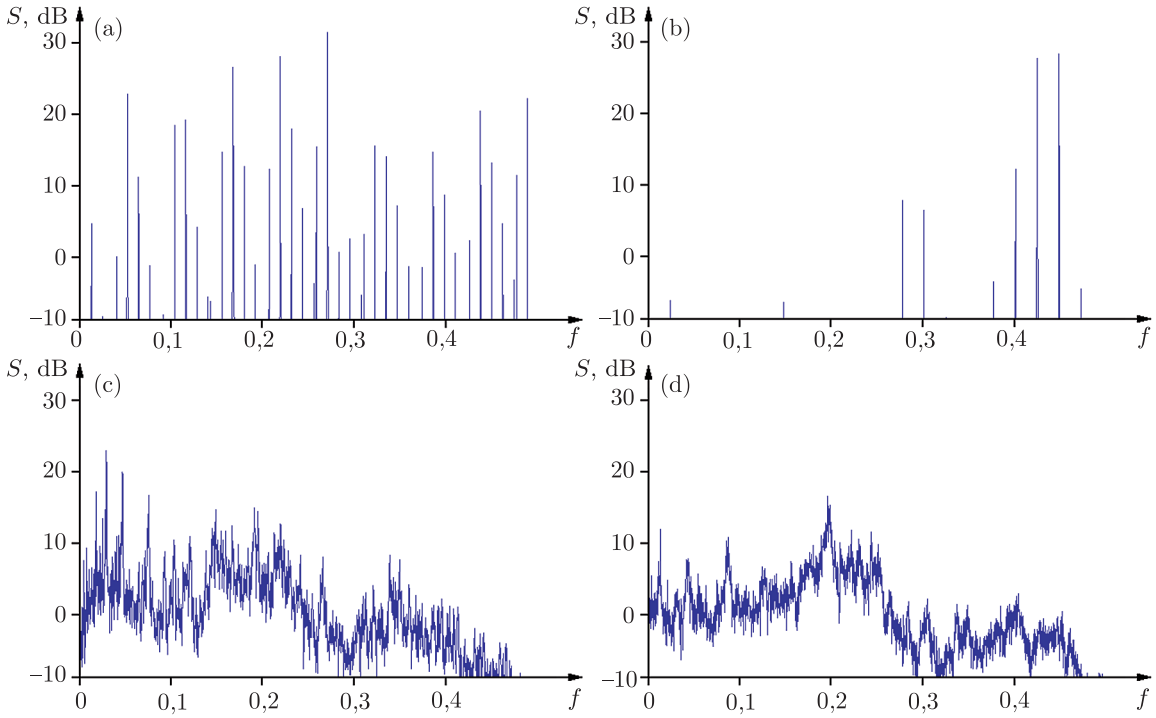

Fig. 10. Power spectra of oscillatory regimes of the system (5.1): (a) 2-frequency quasi-periodic regime at $M = 2.15$, (b) 3-frequency quasi-periodic regime at $M = 3.0$, (c) SNA at $M = 2.0$, (d) chaotic regime at $M = 2.04$.

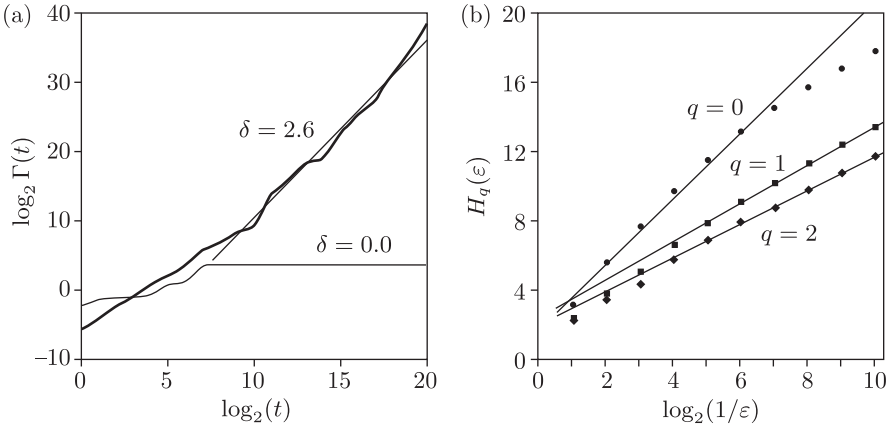

Fig. 11. (a) Plots of the phase sensitivity functions $\Gamma(t)$ for SNA ($\delta = 2.6$) and for 2D torus ($\delta = 0$). (b) The dependence of Renyi entropy $H_q(\varepsilon)$ on the partition scale ε for $q = 0, 1, 2$.

transmitter and the receiver, respectively. In its turn, the idea of using systems with the strange nonchaotic attractor in secure communication schemes has already been expressed, in particular, in [36, 37]. In this context, the designing of systems with strange nonchaotic self-oscillations in a wide range of parameter values is of special interest. Of course, the problem of developing radiotechnical devices with the required properties still remains open. However, the autonomous form of the equations with SNA obtained in this paper, as well as the general idea of converting irrationally related spatial scales to oscillatory modes with incommensurable frequencies essentially expands the class of systems that can exhibit strange nonchaotic dynamics.

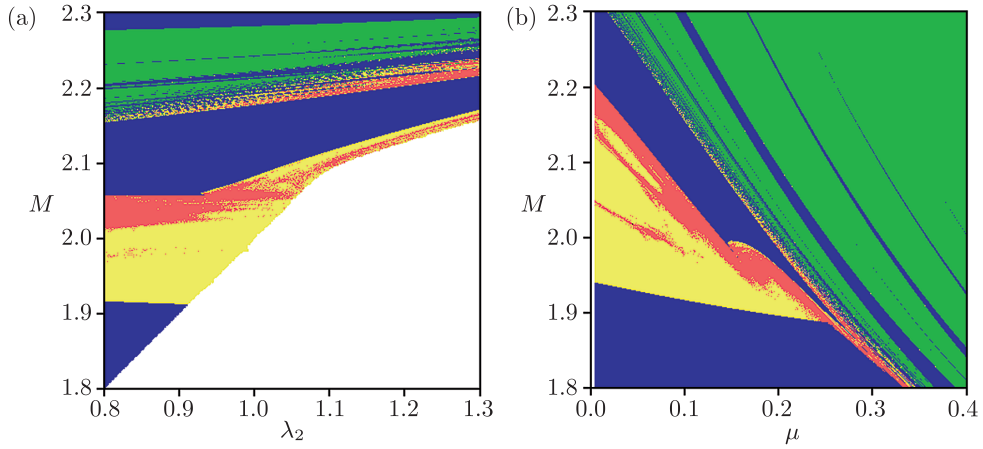

Fig. 12. Fragments of the charts of dynamical regimes of the system (5.1): (a) on the plane (λ_2, M) at $\mu = 0.1$ and (b) on the plane (μ, M) at $\lambda_2 = 0.8$. Two-frequency quasi-periodicity is shown in blue, the three-frequency regime in green, chaos in red, SNA in yellow, and the stable equilibrium point in white.

ACKNOWLEDGMENTS

The work concerning the formulation and simulation of the mechanical model (SPK) was supported by the grant of the Russian Science Foundation No. 15-12-20035 and the work concerning parameter space analysis and computations aimed at detecting and characterizing the SNA (AYuJ) was supported by the grant of the Russian Foundation for Basic Research No. 16-02-00135.

REFERENCES

1. Feudel, U., Kuznetsov, S., and Pikovsky, A., *Strange Nonchaotic Attractors: Dynamics between Order and Chaos in Quasiperiodically Forced Systems,* World Sci. Ser. Nonlinear Sci. Ser. A Monogr. Treatises, vol. 56, Hackensack, N.J.: World Sci., 2006.
2. Ding, M. Zh., Grebogi, C., and Ott, E., Dimensions of Strange Nonchaotic Attractors, *Phys. Lett. A,* 1989, vol. 137, nos. 4–5, pp. 167–172.
3. Hunt, B. R. and Ott, E., Fractal Properties of Robust Strange Nonchaotic Attractors, *Phys. Rev. Lett.,* 2001, vol. 87, no. 25, 254101, 4 pp.
4. Pikovsky, A. and Feudel, U., Correlations and Spectra of Strange Nonchaotic Attractors, *J. Phys. A,* 1994, vol. 27, no. 15, pp. 5209–5219.
5. Feudel, U., Pikovsky, A., and Politi, A., Renormalization of Correlations and Spectra of a Strange Nonchaotic Attractor, *J. Phys. A,* 1996, vol. 29, no. 17, pp. 5297–5311.
6. Pikovsky, A. S., Zaks, M. A., Feudel, U., and Kurths, J., Singular Continuous Spectra in Dissipative Dynamics, *Phys. Rev. E (3),* 1995, vol. 52, no. 1, part A, pp. 285–296.
7. Grebogi, C., Ott, E., Pelikan, S., and Yorke, J. A., Strange Attractors That Are Not Chaotic, *Phys. D,* 1984, vol. 13, nos. 1–2, pp. 261–268.
8. Bondeson, A., Ott, E., and Antonsen, Th. M., Jr., Quasiperiodically Forced Damped Pendula and Schrödinger Equations with Quasiperiodic Potentials: Implications of Their Equivalence, *Phys. Rev. Lett.,* 1985, vol. 55, no. 20, pp. 2103–2106.
9. Ding, M., Grebogi, C., and Ott, E., Evolution of Attractors in Quasiperiodically Forced Systems: From Quasiperiodic to Strange Nonchaotic to Chaotic, *Phys. Rev. A,* 1989, vol. 39, no. 5, pp. 2593–2598.
10. Pikovsky, A. S. and Feudel, U., Characterization of Strange Nonchaotic Attractors, *Chaos,* 1995, vol. 5, no. 1, pp. 253–260.
11. Feudel, U., Kurths, J., and Pikovsky, A. S., Strange Non-Chaotic Attractor in a Quasiperiodically Forced Circle Map, *Phys. D,* 1995, vol. 88, nos. 3–4, pp. 176–186.
12. Kuznetsov, S. P., Pikovsky, A. S., and Feudel, U., Birth of a Strange Nonchaotic Attractor: A Renormalization Group Analysis, *Phys. Rev. E (3),* 1995, vol. 51, no. 3, part A, R1629–R1632.
13. Nishikawa, T. and Kaneko, K., Fractalization of a Torus as a Strange Nonchaotic Attractor, *Phys. Rev. E,* 1996, vol. 54, no. 6, pp. 6114–6124.
14. Glendinning, P., Intermittency and Strange Nonchaotic Attractors in Quasi-Periodically Forced Circle Maps, *Phys. Lett. A,* 1998, vol. 244, no. 6, pp. 545–550.
15. Kim, S.-Y., Lim, W., and Ott, E., Mechanism for the Intermittent Route to Strange Nonchaotic Attractors, *Phys. Rev. E,* 2003, vol. 67, no. 5, 056203, 5 pp.

16. Osinga, H., Wiersig, J., Glendinning, P., and Feudel, U., Multistability and Nonsmooth Bifurcations in the Quasiperiodically Forced Circle Map, *Internat. J. Bifur. Chaos Appl. Sci. Engrg.,* 2001, vol. 11, no. 12, pp. 3085–3105.
17. Kuznetsov, S. P., Torus Fractalization and Intermittency, *Phys. Rev. E (3),* 2002, vol. 65, no. 6, 066209, 13 pp.
18. Kuznetsov, S. P. and Neumann, E., Torus Fractalization and Singularities in the Current-Voltage Characteristics for the Quasiperiodically Forced Josephson Junction, *Europhys. Lett.,* 2003, vol. 61, no. 1, pp. 20–26.
19. Jalnine, A. Yu. and Osbaldestin, A. H., Smooth and Nonsmooth Dependence of Lyapunov Vectors upon the Angle Variable on a Torus in the Context of Torus-Doubling Transitions in the Quasiperiodically Forced Hénon Map, *Phys. Rev. E (3),* 2005, vol. 71, no. 1, 016206, 14 pp.
20. Jalnine, A. Yu., Kuznetsov, S. P., and Osbaldestin, A. H., Dynamics of Small Perturbations of Orbits on a Torus in a Quasiperiodically Forced 2D Dissipative Map, *Regul. Chaotic Dyn.,* 2006, vol. 11, no. 1, pp. 19–30.
21. Jalnine, A. Yu. and Kuznetsov, S. P., On the Realization of the Hunt – Ott Strange Nonchaotic Attractor in a Physical System, *Tech. Phys.,* 2007, vol. 52, no. 4, pp. 401–408; see also: *Zh. Tekh. Fiz.,* 2007, vol. 77, no. 4, pp. 10–18.
22. Ditto, W. L., Spano, M. L., Savage, H. T., Rauseo, S. N., Heagy, J., and Ott, E., Experimental Observation of a Strange Nonchaotic Attractor, *Phys. Rev. Lett.,* 1990, vol. 65, no. 5, pp. 533–536.
23. Vohra, S. T., Bucholtz, F., Koo, K. P., and Dagenais, D. M., Experimental Observation of Period-Doubling Suppression in the Strain Dynamics of a Magnetostrictive Ribbon, *Phys. Rev. Lett.,* 1991, vol. 66, no. 2, pp. 212–215.
24. Zhou, T., Moss, F., and Bulsara, A., Observation of a Strange Nonchaotic Attractor in a Multistable Potential, *Phys. Rev. A,* 1992, vol. 45, no. 8, pp. 5394–5400.
25. Ding, W. X., Deutsch, H., Dinklage, A., and Wilke, C., Observation of a Strange Nonchaotic Attractor in a Neon Glow Discharge, *Phys. Rev. E,* 1997, vol. 55, no. 3, pp. 3769–3772.
26. Yang, T. and Bilimgut, K., Experimental Results of Strange Nonchaotic Phenomenon in a Second-Order Quasi-Periodically Forced Electronic Circuit, *Phys. Lett. A,* 1997, vol. 236, nos. 5–6, pp. 494–504.
27. Bezruchko, B. P., Kuznetsov, S. P., and Seleznev, Ye. P., Experimental Observation of Dynamics Near the Torus-Doubling Terminal Critical Point, *Phys. Rev. E,* 2000, vol. 62, no. 6, pp. 7828–7830.
28. Anishchenko, V. S., Vadivasova, T. E., and Sosnovtseva, O. V., Strange Nonchaotic Attractors in Autonomous and Periodically Driven Systems, *Phys. Rev. E,* 1996, vol. 54, no. 4, pp. 3231–3234.
29. Pikovsky, A. S. and Feudel, U., Comment on "Strange Nonchaotic Attractors in Autonomous and Periodically Driven Systems", *Phys. Rev. E,* 1997, vol. 56, no. 6, pp. 7320–7321.
30. Mitsui, T. and Aizawa, Y., Intermittency Route to Strange Nonchaotic Attractors in a Non-Skew-Product Map, *Phys. Rev. E,* 2010, vol. 81, no. 4, 046210, 8 pp.
31. Jalnine, A. Yu. and Kuznetsov, S. P., Strange Nonchaotic Self-Oscillator, *Europhys. Lett.,* 2016, vol. 115, no. 3, 30004, 5 pp.
32. Goldstein, H., Poole, Ch. P. Jr., and Safko, J. L., *Classical Mechanics,* 3rd ed., Boston, Mass.: Addison-Wesley, 2001.
33. Pikovsky, A. and Politi, A., *Lyapunov Exponents: A Tool to Explore Complex Dynamics,* Cambridge: Cambridge Univ. Press, 2016.
34. Ott, E., *Chaos in Dynamical Systems,* Cambridge: Cambridge Univ. Press, 1993.
35. Lai, Y.-C., Transition from Strange Nonchaotic to Strange Chaotic Attractors, *Phys. Rev. E,* 1996, vol. 53, no. 1, pp. 57–65.
36. Ramaswamy, R., Synchronization of Strange Nonchaotic Attractors, *Phys. Rev. E,* 1997, vol. 56, no. 6, pp. 7294–7296.
37. Zhou, C. and Chen, T., Robust Communication via Synchronization between Nonchaotic Strange Attractors, *Europhys. Lett.,* 1997, vol. 38, no. 4, pp. 261–265.